Rotational dynamics of colloidal spheres probed with fluorescence recovery after photobleaching

M. P. Lettinga[a)]
Teilinstitut Weiche Materie, Institut für Festkörperforschung, Forschungszentrum Jülich, D-52425 Jülich, Germany

G. H. Koenderink,[b)] B. W. M. Kuipers, E. Bessels, and A. P. Philipse
Van't Hoff Laboratory for Physical and Colloid Chemistry, Debye Institute, Utrecht University, Padualaan 8, 3584 CH Utrecht, The Netherlands

(Received 22 October 2003; accepted 5 December 2003)

We report a polarized fluorescence recovery after photobleaching (pFRAP) method to measure the rotational dynamics of fluorescent colloids over a wide dynamic range. The method is based on the polarization anisotropy in the fluorescence intensity, generated by bleaching of fluorescently labeled particles with an intense pulse of linearly polarized laser light. The rotational mobilities of the fluorescent particles can be extracted from the relaxation kinetics of the postbleach fluorescence polarization anisotropy. Our pFRAP setup has access to correlation times over a range of time scales from tens of microseconds to tens of seconds, and is highly sensitive, so very low concentrations of labeled particles can be probed. We present a detailed description of the theoretical background of pFRAP. The performance of the equipment is demonstrated for fluorescent colloidal silica spheres, dispersed in pure solvents as well as in fd-virus suspensions. © *2004 American Institute of Physics.* [DOI: 10.1063/1.1644799]

I. INTRODUCTION

Many experimental studies have been done concerning translational diffusion in concentrated colloidal suspensions, using dynamic light scattering, fluorescence recovery after photobleaching, and nuclear magnetic resonance.[1] Rotational diffusion of colloidal spheres, on the other hand, has received far less attention, partly because options to measure the reorientation of spherical particles are limited. In order to observe the rotational diffusion of a sphere, it needs to have some tag that permits monitoring of its orientation. The first observations of rotational diffusion of colloidal particles were performed by Perrin, who made big spheres (13 μm diameter) out of mastic and gamboge gum with small inclusions of alcohol.[2] This method was successfully used to determine Avogadro's number using the Stokes–Einstein–Debye relation [Eq. (1)], but its applicability is limited by the optical resolution of the microscope. Nowadays the best-known technique to measure rotational diffusion is depolarized dynamic light scattering (DDLS), which requires optically anisotropic colloidal tracer spheres.[3] Although this technique has a wide dynamic range, its applicability is restricted because optically anisotropic spheres are scarcely available. Furthermore, DDLS requires optically matched colloidal systems. These limitations prompted us to initiate the use of time-resolved phosphorescence anisotropy (TPA) for colloids,[4–7] a technique widely used for studying reorientational motions of biological molecules such as muscle proteins.[8] In a TPA experiment, a polarized light pulse (*pump*) creates an anisotropic subset of excited-state fluorophores with absorption dipole moments along the polarization direction. Subsequently, the polarization of the phosphorescence emitted from the excited state decay is monitored.

TPA can be done on fluorophore labeled colloidal particles such as silica spheres, which are much easier to synthesize than the optically anisotropic particles needed for DDLS.[4] An added advantage of TPA is that it can be applied even when the system is somewhat opaque.[5,7] A major drawback of TPA, however, is that the maximum accessible experimental time scale is limited to at most a few ms owing to the finite lifetime of the excited (triplet) state of the dyes. Given the cubic dependence of the rotational diffusion coefficient on the tracer particle radius a_T, according to

$$D_0^r = \frac{k_B T}{8\pi\eta_0 a_T^3}, \tag{1}$$

only a limited range of particle sizes (up to ca. 100 nm) can therefore be measured with TPA. In Eq. (1), η_0 is the solvent viscosity and $k_B T$ is the thermal energy. This limitation motivated us to employ another technique from the field of biomolecules[9–13] to colloids, namely polarized fluorescence after photobleaching (pFRAP).

pFRAP is a so-called *pump-and-probe* technique.[9–13] An anisotropic distribution of unbleached ground-state fluorophores is created by a strong polarized bleach pulse (*pump*) and its orientational relaxation is probed by a much attenuated polarized excitation beam (*probe*). A similar pump-and-probe method is forced Rayleigh scattering (FRS), where a refractive index grating is created by means of an interference pattern, from which grating scattered intensities are

a)Author to whom correspondence should be addressed. Electronic mail: p.lettinga@fz-juelich.de
b)Present address: Physics of Complex Systems, Vrije Universiteit, De Boelelaan 1081, 1081 HV Amsterdam, The Netherlands.

measured.[14] FRAP (and FRS) is applicable to time scales from tens of microseconds up to seconds or more, in contrast to *pump-only* techniques like TPA. pFRAP can be applied even to large particles and/or to very concentrated colloidal suspensions with slow particle dynamics, as we will demonstrate in this paper. The fluorescently labeled tracer particles needed for pFRAP, like those needed for TPA, are relatively easy to synthesize.

Like TPA, pFRAP was originally introduced in the 1980's in a biological context, namely for studying rotational diffusion of lipids in membranes.[9] pFRAP was since then also applied to proteins in biological membranes,[11–13] DNA fragments,[10] and tested on dilute dispersions of latex spheres.[11] In all these cases an epifluorescence microscope geometry was used. Recently, a modified table-top setup was used by Cicerone and Ediger[15,16] to study reorientation of molecular probes in glass-forming materials. Our setup combines features of the two types of setups. Following Cicerone and Ediger,[15,16] we use a specific experimental geometry which ensures that the absorption dipole autocorrelation function is measured, simplifying interpretation of the data compared to the microscope geometry used elsewhere.[10–13] Like Axelrod,[13] we employ short, nanosecond bleach pulses from a pulsed laser and a weak continuous probe beam from a second laser. This allows to study very short, submillisecond, time scale reorientations. In most previous studies the bleach and probe beams originated from the same cw laser and the intensity was modulated by a photoelastic modulator[16] or an acousto-optic modulator,[11,12] giving bleach pulses of milliseconds or more.

The layout of this article is as follows. Section II contains a theoretical treatment of the pFRAP method. Our formalism is more general than that used elsewhere,[9,11,17–20] which has the advantage that it can be applied both to isotropic and aligned phases of spherical and nonspherical particles. We will explain the choice of the experimental geometry and the relation of the measured correlation functions to the rotational diffusion of the dye-labeled colloids. Section III describes the pFRAP experimental setup in some detail and also introduces the fluorescently labeled tracer colloids. In Sec. IV the performance of the pFRAP setup is demonstrated. The influence of experimental parameters like the bleach and probe intensity and the choice of the dye molecule are discussed. We compare TPA and pFRAP measurements on the same eosin-labeled silica tracer spheres. The large dynamic range of pFRAP is demonstrated through measurements of the free rotational diffusion of small colloidal silica spheres ($a_T = 72\,\mathrm{nm}$) at infinite dilution as well as the hindered rotational diffusion of silica spheres in a concentrated dispersion of fd virus rods. Finally, Sec. V contains a summary and conclusions.

II. THEORETICAL BACKGROUND

A. Principle of polarized FRAP

The FRAP experiment is a *pump-and-probe* method. A short intense bleach pulse at time $t=0$ irreversibly quenches the fluorescence of a fraction of the exposed fluorophores by a photochemical reaction. The bleach thereby *pumps* an ensemble of fluorophores from the electronic ground state into a permanent nonfluorescent state. The weak continuous probe (or reading) beam subsequently excites the remaining fluorophores from the ground state to the first excited state. The probe beam thus *probes* the number of molecules that is available in the ground state. The excited state fluorophores relax to the ground state on emitting a fluorescent photon. After the bleach pulse, bleached colloids in the focus of the probe beam will exchange via translational diffusion with unbleached colloids outside. This process gives rise to a recovery of the fluorescence intensity. When unpolarized bleach and probe beams are used, the fluorescence recovery contains information only on the translational dynamics of the fluorescent particles. Instead, when linearly polarized bleach and probe beams are used, the fluorescence recovery additionally reflects the reorientational dynamics of the fluorophores. A linearly polarized bleach pulse creates an anisotropic distribution of bleached (and unbleached) fluorophores, leading to polarization of the excitation process. The polarization anisotropy of the excitation process as probed with a linearly polarized probe beam is gradually lost due to orientational relaxation of the anisotropic ground-state distribution.

In a pFRAP experiment three polarization directions are relevant. The polarization directions of the bleach and probe beams will be denoted by the unit vectors $\hat{B}$ and $\hat{A}$, respectively. The fluorescence emission is observed through a polarizing filter with an orientation denoted as $\hat{E}$. Later, we will specify the experimental geometry.

The fluorescence intensity $I(t)$ measured in a pFRAP experiment is given by

$$I(t) = A(t) C_{\mathrm{exp}} \int d\Omega \int d\Omega_0 \int d\mathbf{r} \int d\mathbf{r}_0 \times R(\mathbf{r}_0, \Omega_0) R(\hat{B}, \Omega, \mathbf{r}; t | \mathbf{r}_0, \Omega_0) P_A(\Omega) P_E(\Omega), \tag{2}$$

where the integration ranges over the orientations and positions of all ground-state dye molecules within the sample volume V illuminated by the probe beam. The constant C_{exp} is a product of the label's quantum efficiencies for photon absorption and emission and the detection efficiency. $R(\hat{B}, \Omega, \mathbf{r}; t | \mathbf{r}_0, \Omega_0)$ is the conditional probability density function (pdf) for dye molecules in the ground state at time t to have positions $\mathbf{r}$ and orientations Ω following a pump pulse at $t=0$ polarized along $\hat{B}$, given that they had positions $\mathbf{r}_0$ and orientations Ω_0 at $t=0$. $R(\mathbf{r}_0, \Omega_0)$ is the equilibrium pdf that the dye molecules have positions $\mathbf{r}_0$ and orientations Ω_0 at $t=0$. In an isotropic system a molecule can be found with equal probability at any given orientation and position, so that $R(\mathbf{r}_0, \Omega_0) = 1/(8\pi^2 V)$.

The orientations Ω are expressed in terms of the three Euler angles α, β, and γ, as explained in Fig. 1. The fluorescence intensity at time t is proportional to the probability $P_A(\Omega)$ of absorption of a probe photon with polarization $\hat{A}$ at time t, and the probability $P_E(\Omega)$ of emission of a photon with polarization $\hat{E}$ at time t. We ignore any delay between photon absorption and subsequent emission, which is justi-

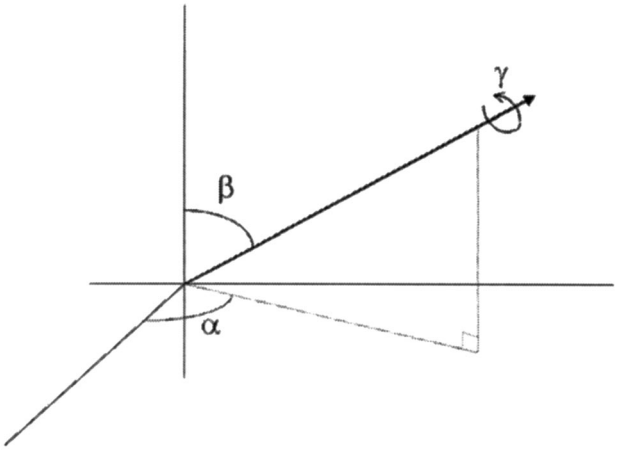

FIG. 1. The coordinate frame used for deriving the pFRAP theory. The orientations $\mathbf{\Omega}$ of the dye molecules are characterized by the three Euler angles, $\Omega \equiv (\alpha,\beta,\gamma)$.

fied by the short (order ns) fluorescence lifetime compared to the experimental time scale of ms to seconds. Finally, $A(t)$ in Eq. (2) accounts for the return of reversibly bleached molecules to the ground state. Apart from irreversible photobleaching, slowly reversible processes[17] like triplet formation may occur.

The bleach changes the pdf of ground-state fluorophores from its initial time-independent distribution $R(\Omega,\mathbf{r})$ to an anisotropic distribution $R(\hat{B},\Omega,\mathbf{r};t|\mathbf{r}_0,\Omega_0)$ that depends on $\hat{B}$

$$R(\hat{B},\Omega,\mathbf{r};t|\mathbf{r}_0,\Omega_0)=R(\Omega,\mathbf{r},t|\mathbf{r}_0,\Omega_0)[1-P_B(\Omega_0)], \tag{3}$$

where $P_B(\Omega_0)$ is the probability that a molecule is bleached at time $t=0$. It is assumed that the bleach pulse is infinitesimally short, so bleaching is instantaneous on the time scale of molecular reorientation. Insertion of Eq. (3) into Eq. (2) gives

$$I(t)\propto I(-)-A(t)\int d\mathbf{r}_0\int d\Omega_0\, R(\mathbf{r},\Omega_0)P_B(\Omega_0) \times\int d\mathbf{r}\int d\Omega\, R(\Omega,\mathbf{r};t|\Omega_0,\mathbf{r}_0)P_A(\Omega)P_E(\Omega), \tag{4}$$

where $I(-)$ is the steady-state fluorescence in absence of a bleach pulse. From here on we will consider the *bleach contrast*

$$\Delta I(t)=I(t)-I(-), \tag{5}$$

i.e., the difference between the recovered intensity after the pulse and the prebleach intensity. Note that $\Delta I(t)$ is negative.

The probabilities of bleaching, photon absorption, and fluorescence emission for a given fluorophore depend on its orientation Ω in the laboratory frame, i.e., its orientation with respect to $\hat{B}$, $\hat{A}$, and $\hat{E}$, respectively. Each fluorophore has absorption and emission transition dipole moments that give the directions of the polarization of the photon for which the probability of absorption or emission is maximal. They are characterized by unit vectors $\hat{\mu}_A$ and $\hat{\mu}_E$ in the frame of the molecule, which are rarely colinear.[21] In the case of rhodamine, the angle between $\hat{\mu}_A$ and $\hat{\mu}_B$ is 23°.[22] The direction of the absorption dipole moment depends on the wavelength of excitation. When the probe and bleach beams have the same wavelength, the corresponding absorption dipole moments $\hat{\mu}_A$ and $\hat{\mu}_B$ are identical. In our experiments the wavelengths of the probe (514.5 nm) and bleach (532 nm) beams are somewhat different, but still within the same excitation band for rhodamine.[22] The probability P_A that a fluorophore absorbs a photon with polarization $\hat{A}$ produced by the probe beam is proportional to

$$P_A(\Omega)\propto|\hat{\mu}_A(\Omega)\cdot\hat{A}|^2. \tag{6a}$$

The probability that a fluorophore emits a photon with a polarization $\hat{E}$ is proportional to

$$P_E(\Omega)\propto|\hat{\mu}_E(\Omega)\cdot\hat{E}|^2. \tag{6b}$$

The probability P_B that a fluorophore is bleached by a photon with polarization $\hat{B}$ produced by the bleach beam is given by $P_B(\Omega_0)=1-\exp[-K|\hat{\mu}_B(\Omega_0)\cdot\hat{B}|^2]$, assuming a first-order bleaching reaction.[18] The parameter $K=C_bI_b\Delta t_b$ is proportional to the bleach pulse intensity I_b and duration Δt_b with a proportionality constant C_b that relates to the efficiency of the bleaching process.[11] In the case of shallow bleaches ($K=1$)

$$P_B(\Omega_0)\cong K|\hat{\mu}_B(\Omega_0)\cdot\hat{B}|^2. \tag{6c}$$

This $\cos^2$ distribution implies a cylindrically symmetric pdf $R(\hat{B},\mathbf{\Omega},\mathbf{r};t)$ about $\hat{B}$ at each position in the illuminated area. In the case of deep bleaches the distribution P_B widens but retains cylindrical symmetry.

As seen in Eq. (4), the time dependence of the fluorescence recovery is determined by the evolution of the pdf, which contains both translational *and* rotational diffusion. The contribution of translational diffusion to the fluorescence recovery depends on the spatial extension of the bleach pattern, i.e., the size of the bleached spot (or the fringe spacing if a grating is bleached), relative to the root-mean-squared displacement $M(\tau^r)=\langle|\mathbf{r}(t)-\mathbf{r}(0)|^2\rangle^{1/2}$ of the particles. The translational diffusion contribution is eliminated when the gradient in the concentration of unbleached particles, $\nabla C(\mathbf{r})$, is negligible on the length scale set by the mean-square displacement $M(\tau^r)$ of the colloidal particle during its typical rotational diffusion time τ^r. The mean-square displacement is typically of the order of the particle dimensions. For instance, in the case of noninteracting spherical particles, $M(\tau^r)$ during a time $\tau^r=1/6D_0^r$ is close to the particle radius, a_T,

$$M(\tau^r)=\sqrt{6D_0^t\tau^r}=\sqrt{\tfrac{4}{3}}a_T, \tag{7}$$

where $D_0^t=k_BT/(6\pi\eta_0a_T)$ is the translational diffusion coefficient. In the more general case of anisotropic diffusion, $M(\tau^r)$ is dominated by the fastest component of the diffusion. If the spatial extension of the bleach pattern is much larger than the particle dimensions, as will be assumed from here on, the contribution of translational diffusion to the

TABLE I. Wigner rotation matrices $D^{\ell}_{mn}(\alpha\beta\gamma)$ of index $\ell=2$ (Ref. 23).

$D^2_{00}(\beta)$	$(3\cos^2\beta-1)/2\equiv P_2(\beta)$
$D^2_{0\pm1}(\beta\gamma)$	$\sqrt{3/2}\sin\beta\cos\beta\exp\{\mp i\gamma\}$
$D^2_{0\pm2}(\beta\gamma)$	$\sqrt{3/8}\sin^2\beta\exp\{\mp 2i\gamma\}$
$D^2_{2\pm2}(\alpha\beta\gamma)$	$\exp\{\mp 2i\alpha\}[(1\pm\cos\beta)/2]^2\exp\{\mp 2i\gamma\}$

fluorescence recovery is negligible, so that $R(\hat{B},\Omega,\mathbf{r};t|\Omega_0,\mathbf{r}_0)$ in Eq. (4) can be set equal to $R(\hat{B},\Omega;t|\Omega_0)$.

Inserting Eqs. (6a)–(c) into Eqs. (4) and (5) leads to the following expression for the bleach contrast:

$$\Delta I(t)=\frac{1}{8\pi^2}A(t)C_{\exp}\langle|\hat{A}\cdot\hat{\mu}_A|^2_t|\hat{E}\cdot\hat{\mu}_E|^2_t|\hat{B}\cdot\hat{\mu}_B|^2_0\rangle, \quad (8)$$

where the angular brackets denote an average over all dye molecule orientations. We assumed that the volumes in the sample illuminated by the bleach and probe beams are identical. Unless the bleach and probe beams originate from the same laser, this is generally not true. However, if the focus volume of the probe is smaller than that of the bleach, as is the case in our setup (see Sec. III A), Eq. (8) remains unchanged.[17]

B. Extracting rotational dynamics from the pFRAP anisotropy

Equation (8) for the bleach contrast contains the time-dependent angles $\Omega_{A\mu_A}$, $\Omega_{E\mu_B}$, and $\Omega_{B\mu_B}$ of the transition dipole moments with the laboratory frame. We are ultimately interested, however, in the orientational dynamics of the colloidal particle, that is, in the time-dependent orientation Ω_{DB} of the colloid in the laboratory frame. Ω_{DB} is the angle of the director $\hat{D}$ of the colloidal particle with the bleach beam direction (i.e., the laboratory frame). In the following we will rewrite Eq. (8) in terms of a correlation function for $\Omega_{DB}(t)$ by a series of coordinate frame rotations. This will be accomplished by employing the Wigner rotation matrices $D^{\ell}_{mn}(\alpha\beta\gamma)$, also known as the generalized spherical functions or D functions.[23] The matrix elements D^{ℓ}_{mn} of the Wigner functions are given explicitly by

$$D^{\ell}_{mn}(\alpha\beta\gamma)=\exp\{im\alpha\}d^{\ell}_{mn}(\beta)\exp\{in\gamma\}, \quad (9)$$

with $\ell=0,1,2,...$; $m,n=-\ell,\ldots,+\ell$. The real functions $d^{\ell}_{mn}(\beta)=D^{\ell}_{mn}(0\beta0)$, which represent a rotation of β about the y axis, are given by

$$d^{\ell}_{mn}(\beta)=\sqrt{(\ell+m)!(\ell-m)!(\ell+n)!(\ell-n)!}\times\sum_k\frac{(-)^k(\cos\beta/2)^{2\ell+m-n-2k}(\sin\beta/2)^{2k-m+n}}{[(\ell+m-k)!(\ell-n-k)!k!(k-m+n)!]}, \quad (10)$$

where the summation runs over values of k for which the arguments of the factorials in the denominator are positive. For the pFRAP theory only the explicit forms of the Wigner rotation matrices of index $\ell=2$ are needed, which are tabulated in Table I. We will furthermore use the closure relation

$$P_2(\beta_{AC})=\sum_{m=-2}^{2}D^2_{0m}(\Omega_{AB})D^2_{m0}(\Omega_{BC}), \quad (11)$$

where $P_2(\beta_{AC})$ is the second-order Legendre polynomial

$$P_2(\beta_{AC})=\tfrac{1}{2}(3\cos^2(\beta_{AC})-1)=\tfrac{1}{2}(3|\hat{A}\cdot\hat{C}|^2-1). \quad (12)$$

Rewriting Eq. (8) with the help of Eq. (12) results in

$$\begin{aligned}\Delta I(t)/(A(t)C_{\exp})\propto 8\langle P_2(\beta^t_{A\mu_A})P_2(\beta^t_{E\mu_E})P_2(\beta^0_{B\mu_B})\rangle&\\ +4\langle P_2(\beta^t_{A\mu_A})P_2(\beta^t_{E\mu_E})\rangle&\\ +4\langle P_2(\beta^t_{A\mu_A})P_2(\beta^0_{B\mu_B})\rangle&\\ +4\langle P_2(\beta^t_{E\mu_E})P_2(\beta^0_{B\mu_B})\rangle&\\ +2\langle P_2(\beta^t_{A\mu_A})\rangle+2\langle P_2(\beta^t_{E\mu_E})\rangle&\\ +2\langle P_2(\beta^0_{B\mu_B})\rangle+1.&\end{aligned} \quad (13)$$

The measured angles $\Omega_{A\mu_A}$, $\Omega_{E\mu_E}$, and $\Omega_{B\mu_B}$ are next resolved into separate components using the closure relation, Eq. (11)

$$P_2(\beta^t_{A\mu_A})=\sum_{m,n,o=-2}^{2}D^2_{0m}(\Omega_{AB})D^2_{mn}(\Omega^t_{BD})D^2_{no}(\Omega^t_{DM})\times D^2_{o0}(\Omega_{M\mu_A}), \quad (14a)$$

$$P_2(\beta^t_{E\mu_E})=\sum_{m,n,o=-2}^{2}D^2_{0m}(\Omega_{EB})D^2_{mn}(\Omega^t_{BD})D^2_{no}(\Omega^t_{DM})\times D^2_{o0}(\Omega_{M\mu_E}), \quad (14b)$$

$$P_2(\beta^0_{B\mu_B})=\sum_{m,n=-2}^{2}D^2_{0m}(\Omega^0_{BD})D^2_{mn}(\Omega^0_{DM})D^2_{n0}(\Omega_{M\mu_B}). \quad (14c)$$

In Eqs. (14a)–(c) we can distinguish time-dependent and time-independent angles. We have the time-independent *experimental angles* Ω_{AB} and Ω_{EB} of the probe and emission polarization directions in the laboratory frame, i.e., with respect to the bleach polarization direction. Additionally, we have time-independent *molecular properties*, namely the angles $\Omega_{M\mu_A}$, $\Omega_{M\mu_E}$, and $\Omega_{M\mu_B}$ of the transition dipole moments in the frame of the molecule. The time-dependent angles are the orientation Ω_{BD} of the *colloid in the lab frame* and the orientation Ω_{DM} of the *fluorophores inside the colloids*. Ω_{BD} is time dependent due to rotational Brownian motion of the colloid, while Ω_{DM} is time dependent due to wobbling of the fluorophores inside the colloid. In the following we will evaluate first the time-independent contributions and next the time-dependent ones.

The absorption and fluorescence dipole moments are situated in the plane of the fluorescent molecule.[22] This implies that the Wigner rotation matrices for $\Omega_{M\mu_A}$, $\Omega_{M\mu_E}$, and $\Omega_{M\mu_B}$ are independent of γ

$$\begin{aligned}D^2_{o0}(\Omega_{M\mu_A})&=D^2_{o0}(\Omega_{M\mu_A})\delta_{o0}\\&=D^2_{00}(\Omega_{M\mu_A})\delta_{o0}\\&=P_2(\beta_{M\mu_A})\delta_{o0},\end{aligned} \quad (15)$$

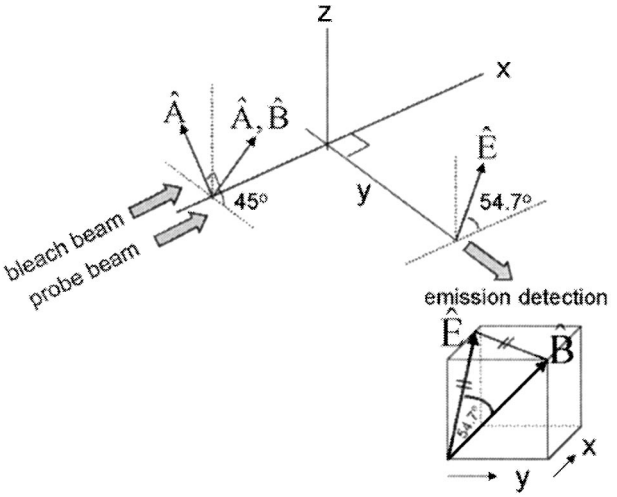

FIG. 2. Sketch of the experimental geometry. The sample is located at the origin, the incoming bleach and probe beams travel along the *x* axis, fluorescence is detected along the *y* axis, and the *z* axis is the vertical direction. The bleach beam ($\hat{B}$) is linearly polarized at an angle $\beta=45°$, the probe beam ($\hat{A}$) is linearly polarized with $\beta=\pm 45°$, and the fluorescence emission passes through a linear polarizer ($\hat{E}$) at an angle $\beta=35.3°$ with the *z* axis and an angle of 54.7° with the *x* axis. The inset cube in the lower right-hand corner shows that both the angle between $\hat{B}$ and $\hat{E}$ and that between the *x* axis and $\hat{E}$ equals 54.7°.

where δ_{n0} is the Kronecker delta. The same can be written for $D^2_{o0}(\Omega_{M\mu_E})$ and $D^2_{n0}(\Omega_{M\mu_B})$. Inserting Eq. (15) into Eq. (14) gives

$$P_2(\beta^t_{A\mu_A}) = P_2(\beta_{M\mu_A}) \sum_{m,n=-2}^{2} D^2_{0m}(\Omega_{AB}) \times D^2_{mn}(\Omega^t_{BD}) D^2_{n0}(\Omega^t_{DM}), \tag{16a}$$

$$P_2(\beta^t_{E\mu_E}) = P_2(\beta_{M\mu_E}) \sum_{m,n=-2}^{2} D^2_{0m}(\Omega_{EB}) \times D^2_{mn}(\Omega^t_{BD}) D^2_{n0}(\Omega^t_{DM}), \tag{16b}$$

$$P_2(\beta^0_{B\mu_B}) = P_2(\beta_{M\mu_B}) \sum_{m=-2}^{2} D^2_{0m}(\Omega^0_{BD}) D^2_{m0}(\Omega^0_{DM}). \tag{16c}$$

The angles $\beta_{M\mu_A}$ and $\beta_{M\mu_E}$ can be experimentally determined by angle-resolved fluorescence depolarization measurements on immobilized molecules in uniaxially stretched polymer films.[22]

The experimental geometry is generally chosen to eliminate the polarization dependence of the fluorescence emission, $D^2_{0m}(\Omega_{EB})$, or the absorption, $D^2_{0m}(\Omega_{AB})$. In the theoretical paper of Wegener[17] on pFRAP various possible geometries are specified. In this work we opt for the geometry sketched in Fig. 2, for which the polarization dependence of the emission will vanish. The bleach and probe beams are directed along the *x* axis, and the fluorescence is detected at right angles to the incoming beams using small-angle collection optics. The sample is contained in a cuvette placed in the origin. Now, to reduce the emission polarization dependence we note that $D^2_{0m}(\Omega_{EB})$ is independent of γ, so that

$$\begin{aligned} D^2_{0m}(\Omega_{EB}) &= D^2_{0m}(\Omega_{EB})\,\delta_{m0} \\ &= D^2_{00}(\Omega_{EB})\,\delta_{m0} \\ &= P_2(\beta_{EB})\,\delta_{m0}. \end{aligned} \tag{17}$$

The term $P_2(\beta_{EB})=(3\cos^2\beta_{EB}-1)/2$ reduces to zero when β_{EB} is 54.7°. This is achieved when the polarization of the bleach beam $\hat{B}$ is kept fixed at an angle $\beta=45°$ from the vertical, while the emission is observed through a polarizing filter along $\hat{E}$, oriented at $\beta=35.3°$ from the vertical. The probe beam is then switched between two polarization modes of $\hat{A}$, namely parallel to $\hat{B}$ ($\beta=45°$) or perpendicular to $\hat{B}$ ($\beta=-45°$) (see Fig. 2).

The geometry sketched in Fig. 2 thus ensures that the fluorescence emission is collected without polarization bias so that the FRAP signal depends only on the absorption dipole orientations. In contrast, the epi-illumination microscopy geometry[11] often used for pFRAP involves horizontal probe and emission directions, the bleach beam is switched between horizontal and vertical, and the fluorescence is observed by a finite aperture objective along the optical axis of the excitation beam. In this case the fluorescence detection is biased and the fluorescence depolarization depends at the same time on the absorption and emission dipole orientations. Accordingly, there will be an additional higher-order rotational relaxation contribution to the anisotropy that decays at a faster rate.[11] An alternative way to eliminate the $D^2_{0m}(\Omega_{EB})$ dependence is to collect all emitted photons without bias using 2π or 4π collection optics.[18]

As stated above, the fluorescence intensity is measured under two experimental conditions, namely $\hat{A}\|\hat{B}$ and $\hat{A}\perp\hat{B}$. We will denote the corresponding bleach contrasts as $\Delta I_{\|}(t)$ and $\Delta I_{\perp}(t)$, respectively. When the bleach and probe polarizations are parallel, $D^2_{0m}(\Omega_{AB})\equiv P_2(\beta_{AB})\,\delta_{m0}$ is equal to $D^2_{0m}(\Omega_{AB})\equiv\delta_{m0}(\cos(\beta_{AB})=1)$. When the bleach and probe polarizations are mutually perpendicular, $D^2_{0m}(\Omega_{AB})\equiv-(1/2)\,\delta_{m0}$. The Legendre polynomial $P_2(\Omega^t_{A\mu_A})$ in Eq. (14a) now has the following form:

$$P_2(\beta^t_{A\mu_A}) = P_2(\beta_{M\mu_A}) \sum_{m=-2}^{2} D^2_{0m}(\Omega^t_{BD}) D^2_{m0}(\Omega^t_{DM}), \quad \text{in the case } \hat{A}\|\hat{B}, \tag{18a}$$

$$P_2(\beta^t_{A\mu_A}) = -\tfrac{1}{2} P_2(\beta_{M\mu_A}) \sum_{m=-2}^{2} D^2_{0m}(\Omega^t_{BD}) D^2_{m0}(\Omega^t_{DM}), \quad \text{in the case } \hat{A}\perp\hat{B}. \tag{18b}$$

For convenience, we will use the closure relation to temporarily make the replacements

$$P_2(\beta^t_{BM}) = \sum_{m=-2}^{2} D^2_{0m}(\Omega^t_{BD}) D^2_{m0}(\Omega^t_{DM}), \tag{19a}$$

$$P_2(\beta^0_{BM}) = \sum_{m=-2}^{2} D^2_{0m}(\Omega^0_{BD}) D^2_{m0}(\Omega^0_{DM}), \tag{19b}$$

in Eq. (18) for $P_2(\beta^t_{A\mu_A})$ and Eq. (16c) for $P_2(\beta^0_{B\mu_B})$, respectively. Note that the ensemble averages $\langle P_2(\beta^t_{BM})\rangle$ and $\langle P_2(\beta^0_{BM})\rangle$ are equal and time independent, since we study equilibrium systems.

Summarizing, all contributions to the bleach contrast containing $P_2(\beta^t_{E\mu_E})$ vanish, while for $P_2(\beta^t_{A\mu_A})$ and $P_2(\beta^0_{B\mu_B})$ we can use Eqs. (18) and Eq. (16c), respectively. Inserting these contributions into Eq. (13) gives the following parallel and perpendicular bleach contrasts:

$$\begin{aligned}\Delta I_{\parallel}(t)/(A(t)C_{\mathrm{exp}}) = {} & 4P_2(\beta_{M\mu_A})P_2(\beta_{M\mu_B}) \\ & \times\langle P_2(\beta^t_{BM})P_2(\beta^0_{BM})\rangle \\ & +[2P_2(\beta_{M\mu_A})+2P_2(\beta_{M\mu_B})] \\ & \times\langle P_2(\beta_{BM})\rangle + 1, \end{aligned} \tag{20a}$$

$$\begin{aligned}\Delta I_{\perp}(t)/(A(t)C_{\mathrm{exp}}) = {} & -2P_2(\beta_{M\mu_A})P_2(\beta_{M\mu_B}) \\ & \times\langle P_2(\beta^t_{BM})P_2(\beta^0_{BM})\rangle \\ & +[-P_2(\beta_{M\mu_A})+2P_2(\beta_{M\mu_B})] \\ & \times\langle P_2(\beta_{BM})\rangle + 1. \end{aligned} \tag{20b}$$

The bleach contrasts are time dependent due to a combination of reversible bleaching [as contained in $A(t)$] and rotational dynamics of the fluorophores. These contributions can be separated by introducing the total bleach contrast

$$\begin{aligned}\Delta I_{\mathrm{tot}}(t) &= \Delta I_{\parallel}(t) + 2\Delta I_{\perp}(t) \\ &= A(t)C_{\mathrm{exp}}[6P_2(\beta_{M\mu_B})\langle P_2(\beta_{BM})\rangle + 3], \end{aligned} \tag{21}$$

and the anisotropy

$$r(t) = \frac{\Delta I_{\parallel}(t) - \Delta I_{\perp}}{\Delta I_{\mathrm{tot}}(t)} = \frac{2P_2(\beta_{\mu_A\mu_B})\langle P_2(\beta^t_{BM})P_2(\beta^0_{BM})\rangle + P_2(\beta_{M\mu_A})\langle P_2(\beta_{BM})\rangle}{2P_2(\beta_{M\mu_B})\langle P_2(\beta_{BM})\rangle + 1}, \tag{22}$$

where we have used the closure relation to write $P_2(\beta_{\mu_A\mu_B}) = P_2(\beta_{M\mu_A})P_2(\beta_{M\mu_B})$.

Equation (22) resembles the anisotropy measured in *pump-only* luminescence experiments such as TPA.[4–7,24] There are two important differences, though. In Eq. (22) the term $P_2(\beta_{\mu_A\mu_B}) = P_2(\beta_{M\mu_A})P_2(\beta_{M\mu_B})$ relates two absorption dipole moments, which are identical when the bleach and probe beams have the same wavelength. In the *pump-only* case an equivalent term relates the absorption and emission dipole moments which are generally not parallel, particularly in the case of TPA.[5] The second difference between *pump-only* and *pump–probe* techniques is that the denominator of $r(t)$ for the *pump-only* case is the total luminescence intensity, whereas for pFRAP it is the total bleach contrast, $\Delta I_{\mathrm{tot}}(t)$. Accordingly, the time window for *pump-only* experiments such as TPA is limited by the luminescence lifetime. The time dependence of the total bleach contrast, on the other hand, is determined solely by reversible photobleaching processes[17] such as triplet formation, as long as translational diffusion is negligible on the experimental time scale. pFRAP measurements can therefore be extended to much longer time scales than TPA measurements.

C. pFRAP on fluorophore-labeled colloids

The time dependence of the anisotropy is fully determined by the rotational dynamics of the fluorophores, contained in the contribution

$$\begin{aligned}&\langle P_2(\beta^t_{BM})P_2(\beta^0_{BM})\rangle \\ &\quad = \sum_{m=-2}^{2}\sum_{n=-2}^{2}\langle\langle D^2_{0m}(\Omega^t_{BD})D^2_{m0}(\Omega^t_{DM})D^2_{0n}(\Omega^0_{BD}) \\ &\qquad \times D^2_{n0}(\Omega^0_{DM})\rangle\rangle, \end{aligned} \tag{23}$$

where we have inserted the closure relation Eq. (19) for $P_2(\beta^t_{BM})$. The rotational dynamics of the fluorophores has two contributions, namely rotation due to overall rotation of the carrier colloid (described by Ω^t_{BD}) and due to wobbling of the fluorophores inside the colloid (described by Ω^t_{DM}). In general, the molecular motion of the dye inside the colloid is orders of magnitude faster than the overall tumbling motion of the particle. It is therefore acceptable to factorize the correlation function in Eq. (23) into a correlation function for Ω^t_{BD} and one for Ω^t_{DM}

$$\begin{aligned}&\langle P_2(\beta^t_{BM})P_2(\beta^0_{BM})\rangle \\ &\quad = \sum_{n=-2}^{2}\sum_{m=-2}^{2}\langle D^2_{0m}(\Omega^t_{BD})D^2_{0n}(\Omega^0_{BD})\rangle \\ &\qquad \times\langle D^2_{m0}(\Omega^t_{DM})D^2_{n0}(\Omega^0_{DM})\rangle. \end{aligned} \tag{24}$$

The separation of time scales between the internal motion of the dye and the overall tumbling of the colloid further implies that on the colloidal time scale (10^{-3}–10^{0} s), the fluorophore has fully explored the space available to it inside the colloid. Accordingly, the orientations Ω_{DM} at time t and time $t=0$ are to a good approximation fully decorrelated on the time scale of the pFRAP experiment

$$\langle D^2_{m0}(\Omega^t_{DM})D^2_{n0}(\Omega^0_{DM})\rangle \cong \langle D^2_{m0}(\Omega^t_{DM})\rangle\langle D^2_{n0}(\Omega^0_{DM})\rangle. \tag{25}$$

The two averages on the right-hand side of Eq. (25) are equal for an equilibrium system. Insertion of Eq. (25) into (24) gives

$$\langle P_2(\beta_{BM}^t)P_2(\beta_{BM}^0)\rangle = \sum_{n=-2}^{2}\sum_{m=-2}^{2}\langle D_{m0}^2(\Omega_{DM})\rangle \times\langle D_{n0}^2(\Omega_{DM})\rangle \times\langle D_{0m}^2(\Omega_{BD}^t)D_{0n}^2(\Omega_{BD}^0)\rangle. \quad (26)$$

When the distribution of fluorophores inside the colloids is cylindrically (or spherically) symmetric, the equilibrium average in Eq. (26) is taken over a pdf that is independent of α, so $D_{m0}^2(\Omega_{DM})$ and $D_{n0}^2(\Omega_{DM})$ can be set equal to $P_2(\beta_{DM})\delta_{m0}$ and $P_2(\beta_{DM})\delta_{n0}$, respectively. Equation (24) thus transforms to

$$\langle P_2(\beta_{BM}^t)P_2(\beta_{BM}^0)\rangle = C_{DM}\langle P_2(\Omega_{BD}^t)P_2(\Omega_{BD}^0)\rangle, \quad (27)$$

where $C_{DM}=\langle P_2(\beta_{DM})\rangle^2 \in [0,1]$ is a constant that depends on the mobility of the fluorophore inside the colloid. When the dye can freely reorient, C_{DM} is zero on the time scale of pFRAP and consequently the anisotropy $r(t)$ is zero. Accordingly, rotational diffusion of labeled colloids can only be measured when the labels are rigidly anchored in the particle. The rapid motion of a fluorophore at its binding site is often treated within a model of isotropic wobbling in a cone.[10,11,17] The wobbling motion and limiting value C_{DM} can be measured with time-resolved fluorescence anisotropy measurements.[5]

At $t=0$ the correlation function $\langle P_2(\Omega_{BD}^t)P_2(\Omega_{BD}^0)\rangle$ reduces to[24]

$$\langle P_2(\Omega_{BD}^0)P_2(\Omega_{BD}^0)\rangle = \tfrac{1}{5}+\tfrac{2}{7}\langle P_2(\beta_{BD})\rangle+\tfrac{18}{35}\langle P_4(\beta_{BD})\rangle, \quad (28)$$

so that the anisotropy at $t=0$ is given by

$$r_0=\frac{2P_2(\beta_{\mu_A\mu_B})C_{DM}\{\frac{1}{5}+\frac{2}{7}\langle P_2(\beta_{BD})\rangle+\frac{18}{35}\langle P_4(\beta_{BD})\rangle\}+\sqrt{C_{DM}}P_2(\beta_{M\mu_A})\langle P_2(\beta_{BD})\rangle}{2\sqrt{C_{DM}}P_2(\beta_{M\mu_B})\langle P_2(\beta_{BD})\rangle+1}. \quad (29)$$

The initial anisotropy r_0 thus depends on the orientation of the absorption dipole moment with respect to the dye, the orientation of the dye with respect to the colloid, and the ordering of the colloids. There are also several experimental factors that affect r_0. When the bleach pulse is deep, the ground-state population becomes depleted for those molecules whose absorption dipole moments are parallel to the bleach polarization $\hat{B}$. Accordingly, the distribution of bleached molecules is broader than the $\cos^2$ distribution in Eq. (6c).[17,18,20] Such saturation effects are expected to become more important when shorter, more intense bleach pulses are used.[20] If the probe beam intersects regions of the sample not illuminated by the pump probe, the fluorescence signal will contain some unwanted background. For shallow bleaches, i.e., to first order in K, the anisotropy is independent of the degree of overlap of the pump and probe beams, but for deep bleaches the anisotropy is reduced by incomplete overlap of the pump and probe beams.[17] We ignored any contributions of scattering to the anisotropy, which decrease the anisotropy when multiple scattering occurs.[25]

D. pFRAP for colloidal spheres

In the case of an isotropic colloidal system the ensemble averages $\langle P_4(\beta_{BD})\rangle$ and $\langle P_2(\beta_{BD})\rangle$ in Eq. (29) vanish, so the final expression for the anisotropy simplifies to

$$r(t)=5r_0\langle P_2(\beta_{BD}^t)P_2(\beta_{BD}^0)\rangle, \quad (30)$$

where r_0 is the initial anisotropy

$$r_0=\tfrac{2}{5}P_2(\beta_{\mu_A\mu_B})C_{DM}\leqslant\tfrac{2}{5}. \quad (31)$$

The correlation function $\langle P_2(\Omega_{BD}^t)P_2(\Omega_{BD}^0)\rangle$, corresponding to the overall tumbling of the colloids, is the only time-dependent contribution to the anisotropy decay on the pFRAP time scale. According to the closure relation we have

$$\langle P_2(\beta_{BD}^t)P_2(\beta_{BD}^0)\rangle=\langle P_2(\hat{D}(t)\cdot\hat{D}(0))\rangle, \quad (32)$$

where the quantity $\hat{D}(t)\cdot\hat{D}(0)$ is the cosine of the angle through which the particle turns in a time t. The functional form of the correlation function depends on the reorientational process. Here, we will recall only the simple case of rotational diffusion of noninteracting, identical spherical Brownian particles, which was first treated by Debye.[26]

The reorientation of a spherical Brownian particle is equivalent to a two-dimensional random walk of the end point of $\hat{D}(t)$ on the surface of a unit sphere. If the particle undergoes many collisions with solvent molecules before it reorients through an appreciable angle, the probability $P(\hat{D},t)d\hat{D}$ for finding a particle with orientation $\hat{D}$ at time t obeys the Debye equation[26]

$$\frac{\partial}{\partial t}P(\hat{D},t)=D_0^r\nabla_\omega^2 P(\hat{D},t), \quad (33)$$

where ∇_ω^2 is the angular part of the Laplace operator ∇^2. The formal solution of the Debye equation is the conditional pdf, $P(\hat{D},t|\hat{D}_0,0)=\exp(tD_0^r\nabla_\omega^2)P(\hat{D},0)$. This pdf corresponds to the probability that the orientation is $\hat{D}$ at time t given the initial condition $P(\hat{D},t=0)=\delta(\hat{D}-\hat{D}_0)$ that it was $\hat{D}_0$ at time $t=0$, with δ the Dirac delta function.[1] Using the orthogonality of spherical harmonics with different indices on the unit sphere and the eigenvalues of the operator $\nabla_\omega^2 Y_{\ell m}(\hat{u})=-\ell(\ell+1)Y_{\ell m}(\hat{u})$, one finds

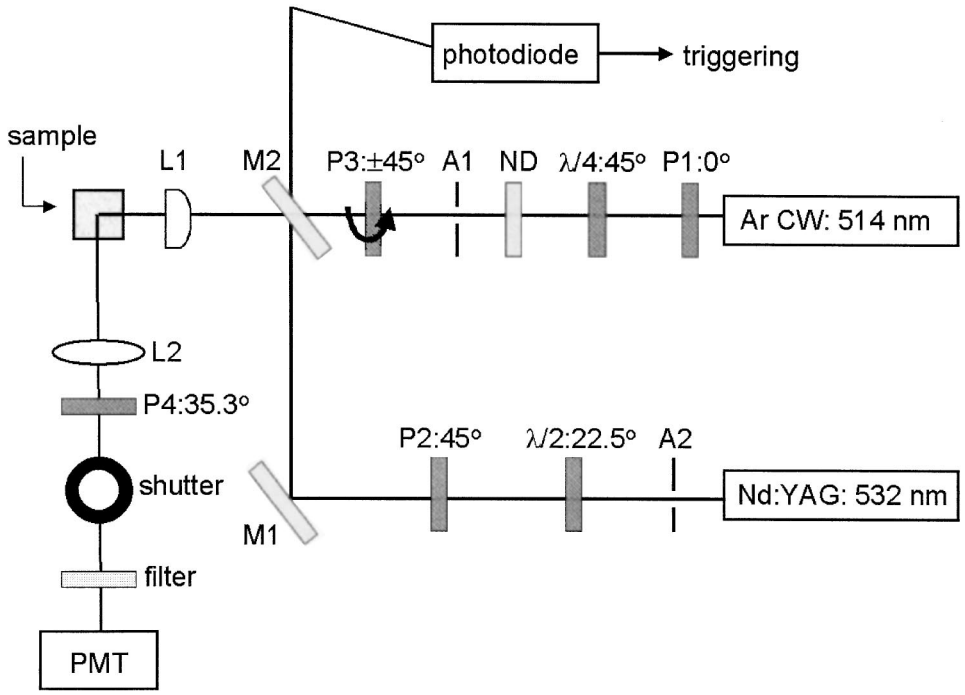

FIG. 3. Schematic depiction of the FRAP setup. Details are explained in the text. Bleach pulses are produced by a Nd-YAG laser and the probe beam originates from an Ar laser. The abbreviations λ/2 and λ/4 denote half-lamda and quarter-lamda platelets; P2 is a Glan-Taylor polarizer; P1, P3, and P4 are sheet polarizers; M1 and M2 are mirrors; L1 and L2 are lenses; A1 and A2 are pinholes, and ND is a neutral density filter. The fluorescence signal is detected with a photomultiplier (PMT), which is protected from scattered and fluorescent light during the bleach pulse with a computer-controlled shutter.

$$P(\hat{u},t|\hat{u}_0,0)=\sum_{\ell,m} Y_{\ell m}(\hat{u}_0)Y^*_{\ell m}(\hat{u})\exp[-\ell(\ell+1)D_0^r t]. \tag{34}$$

In the limit $t\to\infty$ the pdf for an equilibrium ensemble with a uniform distribution of particle orientations is the equilibrium pdf, $P_{\rm eq}(\hat{u})=Y_{00}(\hat{u}_0)Y^*_{00}(\hat{u})=1/4\pi$. Recalling that $r(t)=2P_2(\beta_{\mu_A\mu_B})C_{DM}\langle P_2(\beta^t_{BD})P_2(\beta^0_{BD})\rangle$ for pFRAP, we have the special case $\ell=2$, $m=0$. From the Debye model one can obtain an expression for the orientational correlation function $\langle P_2(\beta^t_{BD})P_2(\beta^0_{BD})\rangle$ by taking the average over the joint probability distribution $P(\hat{u},t;\hat{u}_0,0)=P(\hat{u}_0)P(\hat{u},t|\hat{u}_0,0)$, with $P(\hat{u}_0)=1/4\pi$, and using the relation between spherical harmonics and the Legendre polynomials, $Y_{\ell 0}(\omega)=\sqrt{(2\ell+1)/4\pi}P_\ell(\vartheta)$. Since

$$\langle P_2(\hat{u}_0)P_2(\hat{u}(t))\rangle=\langle P_2(\hat{u}_0\cdot\hat{u}(t))\rangle=\tfrac{1}{5}\exp[-6D_0^r t], \tag{35}$$

the pFRAP anisotropy decay for noninteracting spherical particles reads

$$r(t)=5r_0\langle P_2(\hat{D}(0)\cdot\hat{D}(t))\rangle=r_0\exp(-6D_0^r t), \tag{36}$$

where D_0^r is the Stokes–Einstein–Debye rotational diffusion coefficient specified in Eq. (1). When particle interactions are non-negligible, the decay is slower and generally nonexponential. In the case of nonspherical particles without symmetry the correlation function is more complicated, being a sum of up to five exponentials.[27]

III. EXPERIMENT

A. Instrumental setup

A schematic depiction of the experimental setup is shown in Fig. 3. The pFRAP measurements were performed in a temperature-controlled room at 23 °C. The bleach pulses with a duration of 5 ns are produced by a frequency-doubled Nd-YAG laser (Continuum MiniLite II) with wavelength $\lambda_B=532$ nm and a maximum repetition rate of 10 Hz. The probe beam is produced by a cw Ar–ion laser (Spectra Physics 2000) with wavelength $\lambda_A=514.5$ nm. Both λ_B and λ_A are close to the absorption maximum of rhodamine isothiocyanate (RITC), which is around 560 nm in a silica matrix,[28] and of EosinITC, which is around 530 nm in a silica matrix.[4]

The bleach laser has a vertical polarization ($\beta=0°$). The bleach polarization direction is turned over 45° by a first-order half-wave retardation plate (labeled λ/2 in Fig. 3; Melles-Griot 02WRQ027 for 532 nm), and further optimized with a Glan-Taylor polarizer (labeled P2 in Fig. 3). The bleach beam is directed onto the sample via two mirrors labeled M1 and M2. Mirror M2 is a nonpolarizing broadband beam splitter (OptoSigma 038-0570) with approximately equal reflected and transmitted beams. A reflection of the transmitted beam is directed onto a photodiode, which is used to trigger the oscilloscope (see below). The probe beam is initially vertically polarized ($\beta=0°$). The polarization direction is first optimized with a sheet polarizer (labeled P1). Next, circularly polarized light is created with a quarter-wave retardation plate (labeled λ/4; Melles-Griot 02WRM005 centered at 550 nm). With a thin (0.75 mm) rotatable sheet polarizer (labeled P3; OptoSigma 069-1105 with extinction ratio 10^4) the probe polarization direction $\hat{A}$ is switched between $\beta=\pm45°$. The polarizer is set in a dc-servo motor driven high-speed rotation stage (Newport PR50CC) with accuracy 0.1°, wobble 100 μrad, and a continuous travel range of 360°.

Both the probe and bleach beam are focused to a small spot size within the sample using a fused silica singlet best form laser lens (labeled L1; Melles-Griot with antireflection V-coating) with an effective focal length of 38.1 mm at a wavelength of 532 nm. The spot diameter w_0 is 62 μm for

the bleach beam and 18 μm for the probe beam. The depth of focus, i.e., the distance from the focus where the beam diameter $w=1.05w_0$, is 130 μm for the probe beam and 260 μm for the bleach beam. These conditions ensure that the probe beam falls within the bleach beam, avoiding background fluorescence from unbleached areas. Special precautions were taken during the alignment procedure to make the bleaching and reading beams collinear, by using diffraction patterns generated by a 50 μm pinhole at the sample position. The position of the lens L1 from the sample is optimized to maximize the bleach depth while at the same time taking care that the cuvette is not damaged by the bleach pulse. The typical bleach energy, which can be controlled with an attenuator built in the Nd-YAG laser, was between 0.3 and 1.4 mJ per pulse, as measured with a laser power meter (Ophir Optronics, 3A-P-CAL-SH) placed directly in front of the sample. This corresponds to a peak power of about 200 kW and an intensity of $6.2\cdot10^{27}$ photons/cm$^2\cdot$s. The probe beam intensity is regulated with a neutral-density filter (ND in Fig. 3). Probe powers between 0.04 and 0.3 mW can be used before bleaching due to the probe beam sets in.

The dilute colloidal tracer suspensions were contained in rectangular borosilicate glass vials (Vitrocom CS103) of optical thickness 3×3 mm and length 48 mm. The fluorescent light is detected at right angles to the incident beams, through a sheet polarizer (labeled P4), set at an angle $\beta=35.3°$; see Fig. 2. P4 is actually a component of the fast ferro liquid crystal (FLC) shutter (see below). The fluorescent light is focused onto the PMT (Products For Research, cooled with Peltier to reduce dark current) using a lens (labeled L2). A 607.11 nm bandpass filter (Andover, 600FS40-50; peak transmission 68.2%, FWHM=40 nm) is used to remove scattered excitation light. Additionally, the PMT is protected from scattered light and the luminescence burst excited by the intense bleach pulse by a computer-controlled combination of an electronic gating circuit,[4,5] a fast FLC shutter (Displaytech LV2500AC with Displaytech DR95FLC driver), and a mechanical shutter (Uniblitz VS25S1T0 with VMM-T1 driver/timer). The mechanical shutter is used only in experiments where the sample time exceeds 10 ms. For faster measurements the FLC shutter is used, which consists of a uniaxial birefringent FLC layer between two crossed sheet polarizers. The optical axis of the FLC layer can be electrically switched between two orientations with respect to the first polarizer, namely parallel (closed state) or at 45° (open state). In the open state the FLC layer functions as a half-wave retarder. The shutter has a center wavelength of 550 nm at room temperature, an open shutter transmission of 56%, and a contrast between open/closed transmission of more than 10^3. As shown in Fig. 4, the delay time (for a change from 0 to 10% of the final value) is ~15 μs and the rise time (for a change from 10 to 90% of the final value) is ca. 55 μs. This leads to a total dead time of 70 μs for a pFRAP experiment.

The detected signal from the PMT is amplified with a large dynamic range amplifier (Melles-Griot, 13AMP003) and fed to a digital oscilloscope (LeCroy LT322). A personal computer is used for data collection and controls the timing

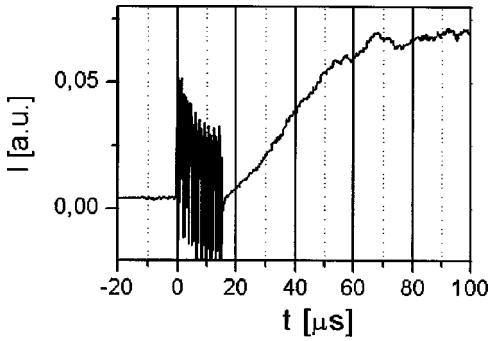

FIG. 4. The switching rate of the FLC shutter is monitored by opening the shutter using a constant probe intensity. The fluorescence intensity $I(t)$ reveals a delay time of ~15 μs and a rise time (for a change from 10% to 90% of the final value) of 55 μs.

of the experiment, through a National Instruments I/O timer card (PC-TIO-10). The translation and rotation stages are controlled via a two-axis integrated controller/driver (Newport Universal Motion Controller ESP300-11N11N, travel of 100 mm, resolution of 1 μm).

B. Data acquisition

To achieve sufficient statistical accuracy, each measurement consisted of several sequences of alternately measuring the fluorescence intensity $I_{\parallel}(t)$, for parallel probe and bleach polarizations, and $I_{\perp}(t)$, for mutually perpendicular probe and bleach polarizations. To accomplish this without waiting for translational diffusion to restore fluorescence to its prebleach value, we used the dc-servo driven translation stage to move the sample down to fresh unbleached spots before each bleaching flash over distances of 150 μm or more. Typically the probe polarization was switched 16 to 32 times and 4 to 32 sweeps were taken each time, giving a total of at least 128 runs per experiment. The rotational diffusion time sets the minimum experimental time per run.

C. Sample preparation and characterization

Silica tracer particles were covalently labeled with either rhodamine B 5-isothiocyanate (RITC), following Verhaegh *et al.*,[28] or with eosin 5-isothiocyanate (EosinITC, following Lettinga *et al.*[5,6] Typical dye contents are 1 dye per $(8\ \text{nm})^3$ to $(13\ \text{nm})^3$ for RITC labeled particles and 1 dye per $(10.5\ \text{nm})^3$ for EosinITC labeled particles. RITC has its excitation maximum around 560 nm and its emission maximum around 580 nm,[28] while EosinITC has its excitation maximum around 530 nm and its emission maximum around 550 nm.[5] Typical extinction coefficients are $2.2\cdot10^4\ \text{M}^{-1}\cdot\text{cm}^{-1}$ at 560 nm ($1.0\cdot10^4\ \text{M}^{-1}\cdot\text{cm}^{-1}$ at 532 nm) for the RITC labeled particles[28] and $7.8\cdot10^4\ \text{M}^{-1}\cdot\text{cm}^{-1}$ at 530 nm for the EosinITC particles.[4,5] All particles consisted of a fluorescent core and a shell of bare silica in order to screen interactions between dye molecules on the surface of the colloid and its environment. In the case of the particles labeled SiSol the total radius was even twice the radius of the fluorescent core.[28] The tracers were dispersed by repeated sedimentation and redispersion in various solvents, including ethanol, water, N,N-dimethylformamide (DMF), dimethylsulfoxide

(DMSO), and a refractive-index matching mixture[6] of DMSO and DMF (3:2 v/v). Rotational diffusion coefficients D_0^r of noninteracting tracers were obtained by diluting the tracer dispersions to volume percentages of 0.01%–0.1%, or a fluorophore concentration of around 0.3 to 3 μM.

The bacteriophage fd is a rod-like molecule with a contour length of $L=880\,\mathrm{nm}$, a diameter of $D_{\mathrm{barc}}=6.6\,\mathrm{nm}$, a persistence length of $P=2200\,\mathrm{nm}$, a molecular weight of $M=1.64\times10^7$ g/mol, and a charge density of 10 e/nm in water at $p\mathrm{H}=8.1$.[29] The fd virus was grown and purified following standard biological protocols,[30] using the XL 1 blue strain of *E. coli* as the host bacteria. The standard yield is ca. 50 mg of fd per liter of infected bacteria, and virus is typically grown in 6-liter batches. The virus particles were purified by repeated centrifugation (10 8000 g for 5 h) and finally redispersed in a 20 mM Tris-HCl buffer at $p\mathrm{H}$ 8.15 with 100 mM NaCl to screen the electrostatic interactions.

D. Heating by bleach pulse

A bleach pulse will locally heat the sample because of light absorption by the fluorophores. The temperature rise, ΔT, at the position of maximum light intensity is bounded above by the expression[10]

$$\Delta T=\frac{9.2\varepsilon CP}{w_0^2\pi c_p\rho}\Delta t, \tag{37}$$

where Δt is the length of the bleach pulse with power P, c_p is the specific heat of the sample, ρ is the solution density, ε represents the extinction coefficient of the dye, C is the fluorophore concentration, and w_0 is the beam waist of the Gaussian intensity profile of the laser. For an experiment on RITC labeled particles at high tracer concentrations (3 μM dye) and high bleaching power (1 mJ laser pulse of 5 ns with a spot diameter w_0 of 62 μm) the local temperature rise will be at most 1.4 °C, taking for the thermal parameters values for amorphous silica.[31] Equation (37) was derived solving the inhomogeneous diffusion equation of heat, using two approximations, both resulting in an overestimate of the maximal bleach-induced temperature increase: the increase in temperature is constant in time, though it is highest at short times; all absorbed photons contribute to the heat production, which means an effective fluorescence quantum yield of zero. One has to consider that all heat is produced within the colloidal particle, so that temperature increase of the surrounding solvent will be even lower. In order to significantly affect the local environment one needs higher extinction coefficients, no fluorescence, and higher laser intensities.

IV. APPLICATION AND DISCUSSION

A. pFRAP on rhodamine-labeled colloidal spheres

A typical example of a pFRAP measurement on rhodamine-labeled colloidal silica spheres is shown in Fig. 5. The sample consisted of SiSol particles ($a_T=230\,\mathrm{nm}$) at a volume fraction of 0.1%, dispersed in DMF. Figure 5(A) displays the time-dependent fluorescence intensities for

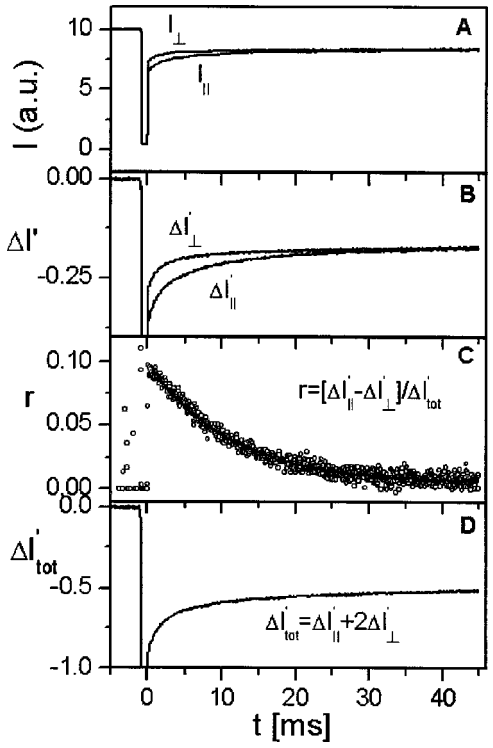

FIG. 5. Photobleaching measurement of the rotational diffusion of rhodamine-labeled SiSol particles ($a_T=230\,\mathrm{nm}$, volume fraction of 0.1%) in DMF. Curves are averages over 128 runs measured at different places in the sample. (A) The fluorescence intensity induced by the probe beam is shown as a function of time. (B) The normalized bleach contrast according to Eq. (38). (C) The anisotropy, with the solid line denoting a best exponential fit. (D) The total normalized bleach contrast.

probe beam polarizations parallel $[I_{\parallel}(t)]$ and perpendicular $[I_{\perp}(t)]$ to the bleach polarization. Figure 5(B) shows the corresponding bleach contrasts

$$\Delta I_{\parallel,\perp}(t)=\frac{\Delta I_{\parallel,\perp}(t)}{I_{\parallel,\perp}(-)}=\frac{I_{\parallel,\perp}(t)-I_{\parallel,\perp}(-)}{I_{\parallel,\perp}(-)}, \tag{38}$$

normalized by the prebleach fluorescence, $I_{\parallel,\perp}(-)$. As seen, ca. 20% of the probe molecules were bleached. Immediately after photobleaching ($t=0$), the magnitude of the parallel bleach contrast $\Delta I'_{\parallel}(0)$ exceeds that of the perpendicular bleach contrast $\Delta I'_{\perp}(0)$, because probe molecules with absorption dipoles parallel to the bleach polarization have been bleached preferentially. In time, rotational Brownian motion of the colloids randomizes the transition dipoles and identical signals are again obtained from both polarizations of the reading beam. Figure 5(C) shows that the anisotropy $r(t)$ decays single exponentially to zero with a characteristic decay time of 10.2 ± 0.2 ms, giving a rotational diffusion coefficient $D_0^r=16\,\mathrm{s}^{-1}$. The initial anisotropy $r_0(t)$ is about 0.1, similar to values reported for colloids with adsorbed dye molecules[11] and for fluorescent molecules in glass-forming liquids.[16]

Figure 5(D) shows the recovery of the total bleach contrast, $\Delta I'_{\mathrm{tot}}(t)$, which contains a slow and a fast recovery. The fast recovery presumably originates from reversibly photobleached molecules in the triplet state returning to the ground state. The slow recovery likely has a contribution of

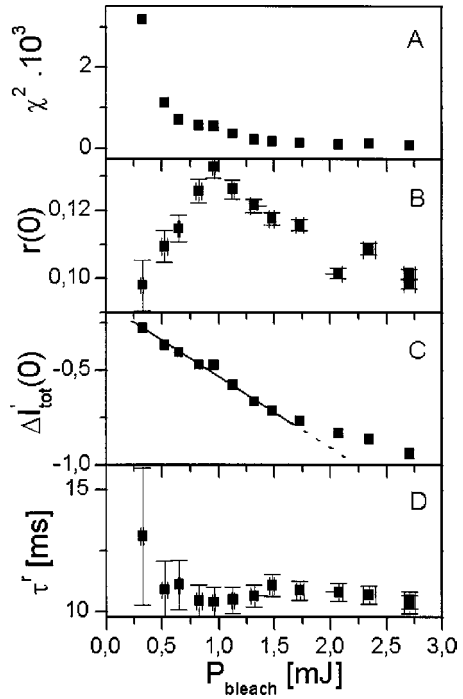

FIG. 6. Effect of bleach intensity on pFRAP measurements performed with the position of the focus at 1.0 mm from the center of the cuvette, containing RITC-labeled SiSol particles ($a_T = 230$ nm, volume fraction 0.1%) in DMF. (A) The χ^2 of the fit of the anisotropy curve decreases with increasing bleach power. (B) The initial anisotropy r_0 first increases with increasing bleach intensity, due to an increasing effective bleach area, and then decreases due to the saturation effect. (C) The total normalized bleach contrast initially depends linearly on the bleach intensity, as assumed in Eq. 6(C), but then flattens, again due to saturation. The solid line is a linear fit to the first points. (D) The rotational diffusion time does not depend on the bleach intensity in the studied range, so the effect of local heating is negligible.

exchange diffusion of bleached particles within the hole and unbleached particles from outside the hole. The fluorescence recovery due to translational diffusion is, however, very small on the experimental time scale, supporting the assumption made in Sec. II that translational diffusion has a negligible contribution to the fluorescence recovery.

B. Influence of bleach intensity

The optimum choice for the probe and bleach power is found by considering several effects. We characterize these effects for our setup by varying the bleach and probe intensity. When the *bleach intensity* is *too low*, the ratio of the signal, due to the bleach, and the noise, due to the fluctuation in the fluorescence intensity, will be low. This can be seen in Fig. 6(A), where the χ^2 error of a single-exponential decay fit is plotted against the bleach intensity. At too-low bleach intensities, also the region where the dye molecules are effectively bleached will be smaller, because of the Gaussian profile of the bleaching beam. Thus, the probe area will be effectively larger than the bleached area, resulting in extra fluorescence that is independent of the polarization of the excitation beam. This leads to a lower contrast between the parallel and perpendicular signal and a reduced initial anisotropy, r_0. This is illustrated in Fig. 6(B), where the anisotropy at $t=0$ is seen to increase initially with bleach intensity.

However, there are limitations to the increase of the laser intensities. *Too-high bleach intensities* may lead to lower anisotropies when the bleach significantly depletes the population of ground-state molecules [see Fig. 6(B)].[20] This effect is also apparent in the bleach intensity dependence of the bleach depth. The bleach depth is linearly dependent on the bleach intensity up to about 1.5 mJ; see Fig. 6(C). This confirms that we are in the range of shallow bleaches ($K=1$) till about 1.5 mJ/pulse, where Eq. (6c) is valid. For higher bleach intensities, the dependence of the bleach depth on the bleach intensity flattens, because the ensemble of bleached molecules is saturated. Too-high bleach intensities may also lead to local heating of the solvent. This effect is expected to induce artificially fast rotational diffusion.[11] However, the measured diffusion coefficients remain constant over the whole range of bleach intensities; see Fig. 6(D), implying that local heating does not affect the viscosity in the range studied.

For the sample discussed above (SiSol in DMF), the optimum bleach intensity is clearly around 1.0 mJ. However, the bleaching efficiency will be reduced when there is a refractive index mismatch between colloid and solvent. If the laser light does not fully penetrate the particle because it is scattered at the particle surface, the effective bleach intensity is reduced and the extinction coefficient of the labeled colloid effectively decreases. Thus, the bleach intensity needs to be optimized for each combination of tracer particle and solvent. Due to refractive index mismatching effects the initial anisotropy r_0 ranges from 0.05 for solvents which are not well matched with silica, in this case ethanol, to 0.182 for the optically matching mixture of DMSO and DMF (3:2 v/v). For particles in water, typical initial anisotropies around 0.1 are found. We note that the phosphorescence lifetime of eosin-labeled silica colloids in water is strongly reduced due to quenching of the excited state, which severely reduces the applicability of TPA to aqueous systems.[5]

A special feature of our experimental setup is that we use a short laser pulse to bleach the sample. Unlike Axelrod *et al.*,[13] who used pulses that were ten times shorter, we find a ''classical'' linear dependence of the bleach depth on the bleach intensity, suggesting a single photon bleaching process. It is, however, remarkable that we use about ten times higher bleach intensities to achieve roughly the same bleach depth. A possible reason for the relatively high bleach intensity may be that the laser beam does not fully penetrate the colloid because it is refracted at the surface. Furthermore, the enhancement of bleaching due to the presence of oxygen is small in the case of our silica spheres since diffusion of oxygen inside the colloids is strongly restricted.[5]

C. pFRAP on eosin-labeled colloidal particles

Figure 7 shows typical pFRAP measurements on eosin-labeled particles dispersed in an optically matching solvent mixture of DMF and DMSO (2:3 v/v). In the following we compare the results with TPA measurements performed on the same system, and pFRAP measurements on rhodamine-labeled SiSol particles, performed under identical conditions.

The bleach depth for eosin-labeled particles is considerable [Fig. 7(A)], in spite of the low bleach intensity of 0.25

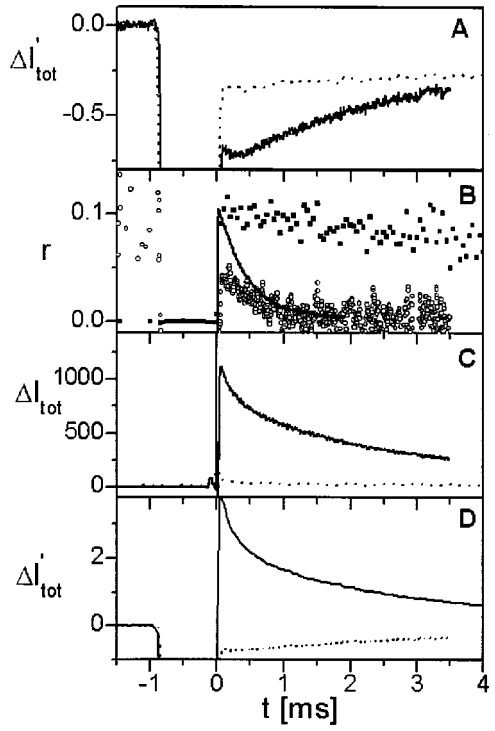

FIG. 7. pFRAP measurement on eosin-labeled particles ($a_T = 72$ nm) dispersed in DMF/DMSO 2:3 v/v and rhodamine-labeled SiSol particles ($a_T = 230$ nm) in DMF, both at a volume fraction of 0.1%. The bleach intensity was 0.25 mJ per pulse. (A) The total normalized bleach contrast for eosin (dotted line) and rhodamine (solid line) particles. (B) The anisotropy for eosin (open symbols) and rhodamine (solid symbols) labeled particles as measured with pFRAP, and of eosin (solid line) as measured with TPA. (C) As in (A) but with the probe beam blocked. (D) The total fluorescence intensity for eosin particles in water (solid line) and dispersed in DMF/DMSO 2:3 v/v (dotted line), showing the important contribution of delayed luminescence when the optical mismatch is large.

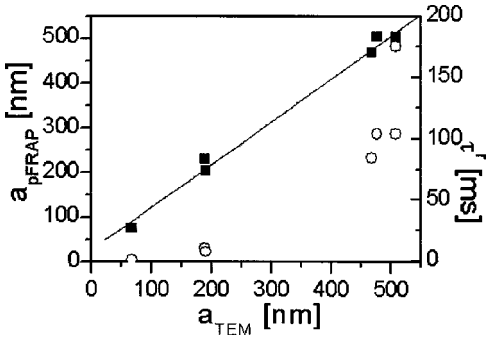

FIG. 8. The hydrodynamic particle radius as determined by pFRAP (closed symbols) plotted versus the bare particle radius, measured with TEM. The pFRAP measurements were performed on rhodamine labeled tracers and on one eosin labeled tracer (smallest radius) dispersed in pure DMF or in DMF/DMSO. Open symbols show corresponding rotational diffusion times, τ_r. The solid line is a linear fit showing that the radius as determined with TEM is always a constant factor smaller than the radius as determined with pFRAP.

mJ-pulse. Interestingly, this deep bleach does not result in a high initial anisotropy r_0 [Fig. 7(B)]. Like for rhodamine-labeled particles, a significant contribution to the decay of the total bleach contrast ΔI_{tot} is due to reversible bleaching [cf. Fig. 5(D)]. The difference between the two dyes is, however, that for rhodamine the reversible photobleaching process is radiation-less, whereas for eosin (and in general for all molecules with a high intersystem crossing rate) there is a relatively high probability that relaxation to the ground state occurs via delayed fluorescence or phosphorescence. The repopulation of the ground state due to a *radiation-less* decay does not affect the anisotropy. The repopulation due to *delayed fluorescence and phosphorescence*, however, results in additional luminescence that is independent of the polarization of the excitation beam. As a result, delayed luminescence causes a blurring of the bleach signal and lowering of r_0.

The difference between eosin and rhodamine-labeled particles is most clearly demonstrated in Fig. 7(C), where the fluorescence signal was detected while the probe beam was blocked. For the rhodamine-labeled particles there is no signal, whereas for the eosin-labeled particles there is a signal with a decay time typical for a delayed luminescence process.[5] The relative contribution of the delayed luminescence very much depends on the optical matching of the tracer particles. This is demonstrated in Fig. 7(A), where the particles are optically matched, and Fig. 7(D), where the particles are dispersed in poorly matching water. In water the large delayed luminescence signal completely overwhelms the bleaching signal. When the refractive index of the tracer is not well matched to that of the solvent, the local laser light intensity in the tracer will be low because the laser is refracted at the surface. When the laser intensity is too low, the dye molecules will not be bleached but pumped into the triplet state instead. For molecules like eosin, which show a strong luminescence decay from the triplet state, this results in a large increase in the luminescence intensity rather than the expected decrease. This effect does not play a role for molecules that do not show delayed luminescence, like rhodamine.

In Fig. 7(B) we also plot the anisotropy decay as measured by TPA, which allows a direct comparison with the pFRAP results. As can be seen, the TPA measurement is far less noisy and the starting anisotropy is significantly higher. The hydrodynamic radius as determined with TPA gives 67.2 ± 0.6 nm, while we find 75 ± 4 nm with pFRAP. Considering the fact that eosin is not a suitable probe for pFRAP, the correspondence is satisfactory. Moreover, we have shown with this comparison that the TPA and pFRAP time windows overlap.

D. Time scales accessible with pFRAP

Figure 8 demonstrates that pFRAP can access a large range of diffusion time scales. Hydrodynamic particle radii a_{pFRAP} measured with pFRAP are plotted as a function of the bare particle radii a_{TEM}, determined by image analysis of TEM micrographs. The pFRAP radii are generally significantly larger than the bare TEM radii. This is also observed for hydrodynamic radii a_{DLS} following from translational diffusion coefficients of silica colloids measured with DLS.[6] TEM radii are generally 5% to 10% smaller than the actual particle radii due to shrinkage of the particles in the electron beam. Additionally, hydrodynamic radii are often larger than the actual radii due to solvation effects, which are especially

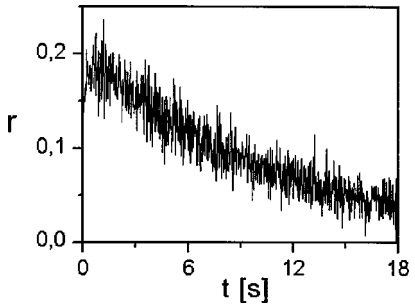

FIG. 9. Orientational relaxation of rhodamine labeled silica ($a_{\mathrm{TEM}}=508$ nm in a dispersion of fd virus rods in a Tris-HCl buffer at pH 8.15 with 100 mM NaCl, at an fd concentration of 4.5 mg/mL. The rotational diffusion time is $\tau^r=12$ s in this dispersion and $\tau^r=0.21$ s at infinite dilution.

important in the solvents DMF and DMSO.[6,7] Taking these effects into account, the overall agreement between a_{pFRAP} and a_{TEM} is quite good.

The range of time scales accessible with pFRAP is even wider than indicated in Fig. 8, where the rotational diffusion times range between 0.4 and 180 ms. The lower limit to the accessible time scales is set by the shutter, which has a dead time of 55 μs (see Fig. 4). For faster decays, TPA can be used, where one can go down to the microsecond range.[5] The upper limit to the accessible time scales is more difficult to define and is probably set by the fact that eventually the probe beam will bleach the particles in the probed area. Unlike TPA, pFRAP can be used to measure slow rotational diffusion processes, such as diffusion of tracer spheres in concentrated dispersions of colloidal host particles.

By way of an example, Fig. 9 shows orientational relaxation of rhodamine-labeled SiSol particles ($a_{\mathrm{TEM}}=230$ nm, $\tau_0^r=0.21$ s) in a concentrated dispersion of fd virus rods in a Tris-HCl buffer with 100 mM NaCl. The fd concentration is 4.5 mg/ml, which is about 100 times the overlap concentration. The rotational diffusion time in the fd dispersion is 60 times larger than at infinite dilution (0.21 versus 12 s). This experiment shows that we can study the influence of a host matrix on the rotational diffusion of immersed tracer spheres over a wide range of host particles concentrations.

V. CONCLUSIONS

In summary, we have shown experimentally and theoretically that pFRAP allows measurements of very slow (up to seconds) rotational diffusion processes in colloidal suspensions. An anisotropic distribution of unbleached ground-state fluorophores is created by a strong polarized bleach pulse (''*pump*'') and the orientational relaxation is probed by a much attenuated polarized excitation beam (''*probe*''). Our setup allows measurement of rotational diffusion times from tens of seconds down to tens of microseconds, since we use a pulsed laser and a very fast shutter in front of the detector. FRAP is very sensitive to low fluorescence intensities and therefore requires only small tracer concentrations. Unlike TPA, FRAP is a destructive technique since it irreversibly destroys the fluorescent molecules within the illuminated volume. The main advantage of pFRAP over TPA is that pFRAP probes the relaxation of an anisotropic ground-state population, while TPA probes excited state molecules. While TPA is limited to a few milliseconds owing to the limited triplet state lifetime, pFRAP allows measurement of recovery dynamics over indefinitely long times owing to the irreversible nature of the photobleaching reaction.

ACKNOWLEDGMENTS

We thank N. A. M. Verhaegh, J. E. G. J. Wijnhoven, C. M. van Kats, A. van Blaaderen, and G. Bosma for providing rhodamine-labeled silica spheres, and J. K. G. Dhont for helpful discussions. S. Sacanna is thanked for contributing supporting pFRAP measurements.

[1] B. J. Berne and R. Pecora, *Dynamic Light Scattering* (Wiley, New York, 1976); J. K. G. Dhont, *An Introduction to Dynamics of Colloids* (Elsevier, Amsterdam, 1996).
[2] J. Perrin, *Atoms* (Constable, London, 1916).
[3] V. Degiorgio, R. Piazza, and R. B. Jones, Phys. Rev. E **52**, 2707 (1995); G. H. Koenderink and A. P. Philipse, Langmuir **16**, 5631 (2000).
[4] M. P. Lettinga, C. M. Van Kats, and A. P. Philipse, Langmuir **16**, 6166 (2000).
[5] M. P. Lettinga, M. A. M. J. Van Zandvoort, C. M. Van Kats, and A. P. Philipse, Langmuir **16**, 6156 (2000).
[6] G. H. Koenderink, M. P. Lettinga, and A. P. Philipse, J. Chem. Phys. **117**, 7751 (2002).
[7] G. H. Koenderink, D. G. A. L. Aarts, and A. P. Philipse, J. Chem. Phys. **119**, 4490 (2003).
[8] S. Ramachandran and D. D. Thomas, Biochemistry **38**, 9097 (1999).
[9] L. M. Smith, R. M. Weis, and H. M. McConnell, Biophys. J. **36**, 73 (1981).
[10] B. A. Scalettar, P. R. Selvin, D. Axelrod, J. E. Hearst, and M. P. Klein, Biophys. J. **53**, 215 (1988).
[11] M. Velez and D. Axelrod, Biophys. J. **53**, 575 (1988).
[12] M. Velez, K. F. Barald, and D. Axelrod, J. Cell Biol. **110**, 2049 (1990).
[13] D. Axelrod, J. L. Rubinstein, and Y. Yuan, Polym. Prepr. (Am. Chem. Soc. Div. Polym. Chem.) **33**, 755 (1992); Y. Yuan and D. Axelrod, Biophys. J. **69**, 690 (1995).
[14] J. Kanetakis and H. Sillescu, Chem. Phys. Lett. **252**, 127 (1996).
[15] M. T. Cicerone and M. D. Ediger, J. Chem. Phys. **97**, 2156 (1992); M. T. Cicerone, F. R. Blackburn, and M. D. Ediger, *ibid.* **102**, 471 (1995); M. T. Cicerone and M. D. Ediger, *ibid.* **103**, 5684 (1995).
[16] M. T. Cicerone and M. T. Ediger, J. Phys. Chem. **97**, 10489 (1993).
[17] W. A. Wegener, Biophys. J. **46**, 795 (1984).
[18] W. A. Wegener and R. Rigler, Biophys. J. **46**, 787 (1984).
[19] R. E. Dale, Eur. Biophys. J. **14**, 179 (1987); M. M. Timbs and N. L. Thompson, Biophys. J. **58**, 413 (1990).
[20] E. H. Hellen and T. P. Burghardt, Biophys. J. **66**, 891 (1994).
[21] J. R. Lakowicz, *Principles of Fluorescence Spectroscopy*, 2nd ed. (Kluwer Academic/Plenum, New York, 1999).
[22] M. A. M. J. Van Zandvoort, D. L. J. Vossen, G. Van Ginkel, R. Torre, P. Bartolini, M. Ricci, J. Thomas-Oates, and H. Zuilhof, Phys. Chem. Chem. Phys. **1**, 4571 (1999).
[23] M. E. Rose, *Elementary Theory of Angular Momentum* (Wiley, New York, 1957); A. R. Edmonds, *Angular Momentum in Quantum Mechanics* (Princeton University Press, Princeton, 1960); C. G. Gray and K. E. Gubbins, *Theory of Molecular Fluids* (Clarendon, Oxford, 1984).
[24] C. Zannoni, Mol. Phys. **38**, 1813 (1979).
[25] F. W. J. Teale, Photochem. Photobiol. **10**, 363 (1969).
[26] P. Debye, *Polar Molecules* (Dover, New York, 1929).
[27] T. J. Chuang and K. B. Eisenthal, J. Chem. Phys. **57**, 5094 (1972); M. Ehrenberg and R. Rigler, Chem. Phys. Lett. **14**, 539 (1972).
[28] N. A. M. Verhaegh and A. Van Blaaderen, Langmuir **10**, 1427 (1994).
[29] S. Fraden, in *Observation, Prediction, and Simulation of Phase Transitions in Complex Fluids*, edited by L. F. R. M. Baus and J. P. Ryckaert (Kluwer Academic, Dordrecht, 1995), Vol. NATO-ASI-Series C, Vol. 460.
[30] J. Sambrook, E. F. Fritsch, and T. Maniatis, in *Molecular Cloning: A Laboratory Manual* (Cold Spring Harbor Laboratory, 1989).
[31] P. W. Atkins, *Physical Chemistry*, 3 ed. (Oxford University Press, Oxford, 1986).